Scripta Materialia 108 (2015) 100–103

Contents lists available at ScienceDirect

Scripta Materialia

journal homepage: www.elsevier.com/locate/scriptamat

The role of shear strain on texture and microstructural gradients in low carbon steel processed by Surface Mechanical Attrition Treatment

Jordan Moering [a], Xiaolong Ma [a], Guizhen Chen [b], Pifeng Miao [b], Guozhong Li [b], Gang Qian [b], Suveen Mathaudhu [c], Yuntian Zhu [a,d,]*

[a] Department of Materials Science and Engineering, North Carolina State University, Raleigh, NC 27695, USA
[b] Jiangyin Xingcheng Special Steel Works Co., Ltd., Jiangyin, Jiangsu, China
[c] Department of Mechanical Engineering, University of California, Riverside, CA, USA
[d] School of Materials Science and Engineering, Nanjing University of Science and Technology, Nanjing, China

ARTICLE INFO

Article history:
Received 24 April 2015
Revised 11 June 2015
Accepted 16 June 2015
Available online 18 June 2015

Keywords:
Shear strain
Gradient
Texture
Microstructure
Hardness

ABSTRACT

In this study, the shear strain at various depths of a low carbon steel processed by Surface Mechanical Attrition Treatment (SMAT) was measured using deformed carbide bands as internal strain markers. The shear strain gradient is found to strongly correlate with the gradients of texture, microstructure and hardness. The microhardness increases approximately linearly with shear strain, but deviates at the top surface. In the top surface, the average ferrite grain size is reduced to 60 nm with a strong {1 1 0}//SMAT surface texture.

Gradient structures are known to produce a wide variety of interesting properties including improved wear resistance and fatigue life, and extraordinary mechanical properties [1–6]. In recent years, Surface Mechanical Attrition Treatment (SMAT) has gained attention for its ability to generate gradient structured materials through grain refinement of the surface layer to the nanometer scale [1,7–10]. This technique is ideal for systematic investigations of gradient structures due to the gradients in strain, strain rate, hardness, grain size, and hardening mechanisms throughout the deformed layer. In order to refine grain sizes to the nanometer scale, large strains and strain rates need to be applied [11–13]. It is well known that the shear component of the applied strain is directly correlated with dislocation slip and microstructure evolution. However, quantitatively mapping a single component of the strain tensor is challenging [14–16]. Markers and photographic evidence have been reported to extract the effect of shear strain on microstructure evolution, but they are not suitable for measuring shear strain in SMAT, due to the complexity of the process [17–19].

In this work, cementite bands are used as internal markers to quantify the shear strain at various depths of the surface, which is the first time shear strain has been quantitatively mapped in SMAT-processed samples. Additionally, the texture evolution is systematically characterized, which has rarely been studied in SMAT-processed structures but profoundly affects mechanical behavior [20–23]. The observations from this work elucidate the effect of shear strain on the development of texture gradient, microstructure gradient, and microhardness gradient in the SMAT-processed samples.

Normalized steel plates with a composition of 0.14% C, 0.33% Si, 1.44% Mn, 0.08% Cr, 0.03% Ni, and balance Fe was used for this study. Samples were cut along the rolling direction so that the SMAT treatment would take place normal to the rolling direction. The pearlite was agglomerated into bands normal to the SMAT surface as shown in Fig. 1. The SMAT process was carried out using a SPEX 8000M Mixer/Mill by replacing the lid of the vial with 1/4″ thick plates of the sample to be treated. Samples were polished to 1200 grit, sealed in ambient atmosphere, and processed with three ½″ 440C steel balls for 120 min. Profilometry revealed that the surface was roughened to an Ra of 8.8 μm. After treatment, cross-sectional samples were Ni-plated to protect the surface microstructure from edge rounding when polishing, and were imaged using a JEOL 6010LA Scanning Electron Microscope (SEM) at 20 kV.

Experimentally measuring a single component of the strain tensor is not a trivial matter. Attempts to discern the shear component

* Corresponding author at: Department of Materials Science and Engineering, North Carolina State University, Raleigh, NC 27695, USA.

E-mail address: ytzhu@ncsu.edu (Y. Zhu).

http://dx.doi.org/10.1016/j.scriptamat.2015.06.027
1359-6462/

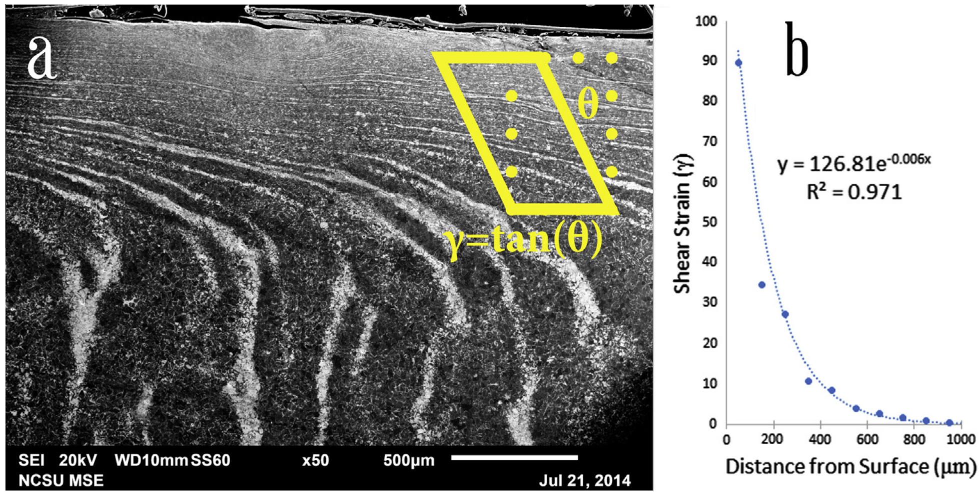

Fig. 1. (a) An SEM image of the as-received SMAT surface. The inset shows how the slope of the cementite bands was measured in order to calculate shear strain γ. (b) The resulting data calculated at various depths showing a clear exponential increase in shear strain approaching the surface of the SMAT gradient.

of the tensor in severe plastic deformation processes have been undertaken primarily by simulation or calculation [11,14,16,18]. Experimentally, an imbedded pin method has been used to measure shear in accumulated roll bonding, where the interface of the pin can be used to map the shear strain, but this is not suitable for SMAT structures [19]. In normalized low carbon steels, clear bands of pearlite along the rolling direction (α-iron + Fe_3C) and ferrite (α-iron) naturally act as markers in the microstructure. Since the plates were cut normal to the rolling direction, these bands were perpendicular to the SMAT surface, as shown in Fig. 1. Because the shot impacts from SMAT repeatedly induce plastic flow in the surface, the top deformed layer is theorized to undergo high shear strains [1,17]. Therefore, simply mapping the slope of the deformed pearlite bands could yield the accumulated shear strain induced at various depths of the SMAT surface. First, a grid with 100 μm blocks was overlayed onto the micrograph seen in Fig. 1A. Then, the average slope was measured in each of these regions to calculate the average shear strain at various depths. In this way, the shear strain plotted at 50 μm, 150 μm, 250 μm, etc. represents the average shear strain at each 100 μm interval. The result indicates that the shear strain increases exponentially near the surface, which is visually apparent in the cross-sectional SEM micrograph (Fig. 1A). A simple exponential fit ($R^2 = 0.97$) was applied to the data in order to estimate the shear strain at discrete depths from the surface. Extrapolation of this data was used to estimate the shear strain at depths less than 100 μm but it is not clear how big the error is from such an extrapolation (Fig. 2). Surprisingly, the average measured shear strain at a depth of 50 μm is 90, and the extrapolated shear strain in the top 10 μm is 119, which is in the realm of shear strains measured in accumulated roll bonding and chip processing, as well as high pressure torsion [14,18,19]. Note that in the very top surface, e.g. at layer thickness close to the roughness, the current strain measurement may significantly underestimate the shear strain.

Once the shear strain was calculated, grain size and microhardness measurements could be plotted to determine their relationship. Five hardness measurements were averaged at each depth with a Mitutoyo Microhardnss Testing Machine Model HM-11 with a Vickers diamond indenter at a load of 0.05 N. Grain size measurements were performed using the line intercept method from micrographs collected from the dual Beam FEI Quanta 3D FEG, the JEOL 2010 F Transmission Electron Microscope. Fig. 2 shows these relationships and a corresponding FIB micrograph of the gradient structure at the surface. Both hardness and grain size show a strong dependency on the shear strain, and the Hall–Petch plot shows slight deviation from the ideal linear trend.

At the top surface, the grain size is dramatically reduced to 60 nm, as seen in Fig. 3. TEM samples confirmed that the grain size at the top surface was skewed, with some regions containing grains less than 10 nm, while other regions had grains 100 nm in diameter. Fig. 3 shows the distribution of grain size at the top 10 μm of the SMATed surface. In carbon steels, nanocrystallization has been reported in regions subject to very high shear strains, and were first discovered in railroad tracks [14]. These regions were called "white etching layers", which consist of fragmented Fe_3C and even complete Fe_3C dissolution that leads to supersaturation of carbon in nanocrystalline α-iron [6,15,24]. These reports are consistent with this observation here.

Because SMAT is a complex deformation scheme consisting of compressive and shear strains at various strain rates, mapping the texture allows for a simple investigation on the underlying deformation schemes at various depths from the surface [1,23]. Samples were prepared for EBSD imaging by conventional polishing followed by ion milling in a Fischione Ion Mill (Model-1060) at 5 kV and 5° tilt for 45 min. An Oxford EBSD detector installed in the dual Beam FEI Quanta 3D FEG was used for collecting images. Fig. 4 shows an overview of the microstructural and textural development along the depth. The as-received material consists primarily of high-angle grain boundaries (>15°) and displays no strong texture. After SMAT, at 200 μm below the surface, no strong texture can be determined, but the grain size has been reduced and clear subgrain boundaries (>2°) can be seen within large grains. At 100 μm below the surface, there is a clear transition to a complex texture with {1 1 0} and some {1 1 1} planes//SMAT surface, and low-angle grain boundaries have evolved from the subgrain boundaries. At 50 μm below the surface, although some residual {1 1 1}//SMAT surface texture can still be seen, the texture mostly transitioned to {1 1 0}//SMAT surface, which is a well-known texture for highly sheared α-iron [21,23]. At the top surface, the {1 1 0}//SMAT surface texture is further strengthened, and most grain boundaries have been converted to high angle. As can be seen in Fig. 4, the development of the texture of {1 1 0}//SMAT surface is preceded by diminishing {1 1 1} components from the depth of 100 μm to the surface.

Texture develops when preferred crystallographic orientations align with applied stress. Slip systems tend to align with the shear direction to maximize the resolve shear stress [1,22]. In BCC α-iron,

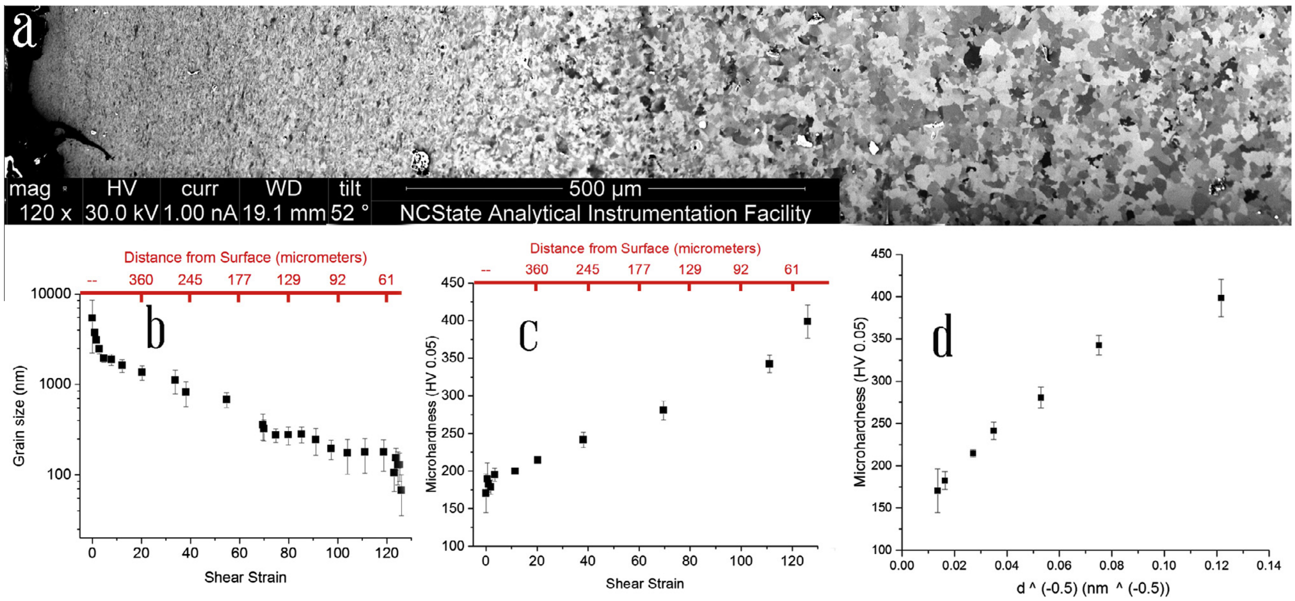

Fig. 2. (a) A cross sectional FIB image of the SMAT gradient extending to depths greater than 500 μm, (b) the strong linear dependence of microhardness on shear strain, (c) the dependence of grain size on shear strain, and (d) the microhardness approximately follows the Hall–Petch relationship.

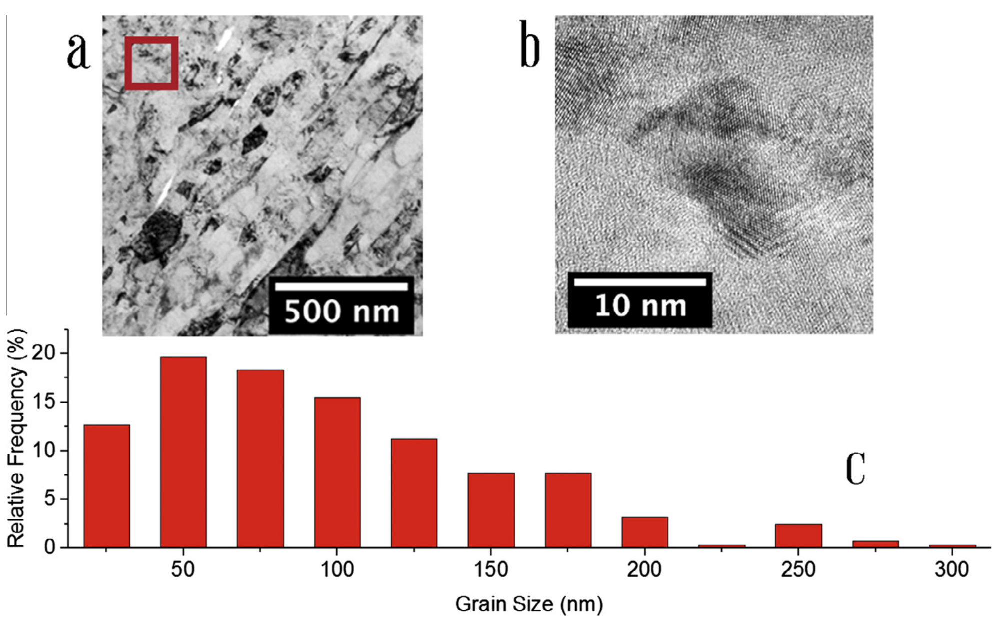

Fig. 3. (a) A representative image of the top surface shows regions with both nanocrystalline (<100 nm) grains and coarser grains intermixed. (b) High resolution TEM of the nanocrystalline region shows a single grain ~10 nm in diameter. This microstructure has been reported in steels subject to high shear strains and indicates partial decomposition of Fe_3C. (c) Grain size distribution at the top surface.

{1 1 0} are the slip planes, and ⟨1 1 1⟩ are the slip directions, so the {1 1 0} ⟨1 $\bar{1}$ 1⟩ slip systems are preferred. When shear is induced during plastic deformation, the resolved shear stress is maximized when the {1 1 0} lie parallel to the shear direction, like a deck of cards. This is why the ⟨1 1 0⟩ α wire texture is commonly found in HPT, wire drawing, and other deformation modes that induce high shear strains [18,13,20].

The SMAT has also induced nanocrystalline regions with grain sizes less than 10 nm as seen in Fig. 3, suggesting the formation of the ⟨1 1 0⟩ α wire texture is accompanied with the dissolution of Fe_3C.

The {1 1 0}//the surface texture was developed through dislocation slip and generation of geometrically necessary dislocations. At the same time, dislocation accumulation and interactions formed subgrain boundaries, which were eventually transformed to high angle grain boundaries, as is consistent with previous reports [1,6–10,23]. These defect structures serve not only to accommodate strain but also to orient the crystallographic directions towards the highest shear directions. The texture, however, is strongest only in the top 100 μm, while grain refinement and shear strain accumulation are also prevalent at depths >350 μm. In these regions, the lack of a strong shear direction may be the reason for the weakness of the texture. Cementite thinning and fragmentation may also play a role. It is clear, however, that the texture forms over a gradient, and is most strongly formed at the highest shear strains with the most severe grain refinement.

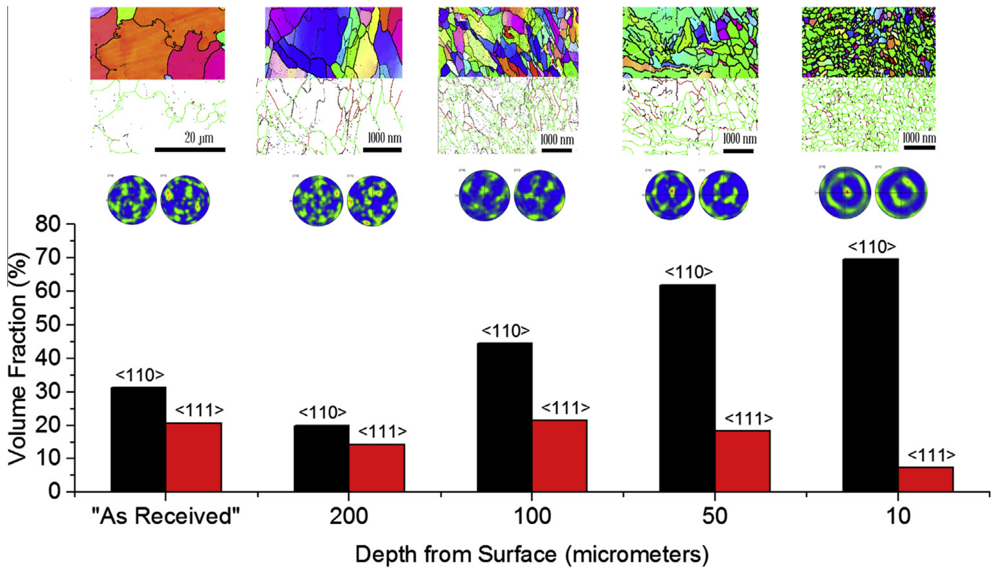

Fig. 4. Development of microstructure and texture at varying depths from the surface. The percentage of grains indexed normal to the SMAT surface were calculated from EBSD maps and show the relative frequency of the {1 1 1}, {1 1 0} and planes in ferrite at various depths. Grain boundary maps indicate high angle (>15°) grain boundaries in green, low angle (<15°) grain boundaries in red, and subgrain (>2°) boundaries in black. Pole figures are projected normal to the SMAT surface, indicating a strong {1 1 0}// SMAT surface texture developed in the top 50 μm. (For interpretation of the references to color in this figure legend, the reader is referred to the web version of this article.)

Because the gradient texture will locally affect deformation mechanics, it will likely plays a role in the global deformation of the sample. For example, the texture gradient will lead to a deformation gradient, which causes macroscopic mechanical incompatibility that has been shown to increase mechanical strength and ductility simultaneously in similar systems [2–4]. Further investigation on the affects of gradient textures and their global response to mechanical stress could provide insight to the exciting developments in gradient structured materials.

In summary, SMAT imparted very large shear strain near the sample surface, which decreases along the depth, which resulted in gradients in hardness, grain size and texture. Fe_3C dissolution occurred near the surface, which helped with the reduction of grain size to 10 nm in local areas. {1 1 0}//SMAT texture was produced over a depth of 100 μm, below which the texture is complex. Further investigation on the effects of gradient textures and their global response to mechanical stress is needed to provide insight to the exciting developments in gradient structured materials.

Acknowledgments

This work is funded by the Jiangyin Xingcheng Special Steel Works Co., Ltd., Jiangsu, China. The authors acknowledge the use of the Analytical Instrumentation Facility (AIF) at North Carolina State University, which is supported by the State of North Carolina and the National Science Foundation. Y.T.Z. also acknowledges the support of the China Thousand Talents Plan.

References

[1] K. Lu, J. Lu, Mater. Sci. Eng. A 375–377 (2004) 38.
[2] T.H. Fang, W.L. Li, N.R. Tao, K. Lu, Science 331 (2011) 1587.
[3] X.L. Wu, P. Jiang, L. Chen, F.P. Yuan, Y.T.T. Zhu, Proc. Natl. Acad. Sci. USA 111 (2014) 7197.
[4] X.L. Wu, P. Jiang, L. Chen, J.F. Zhang, F.P. Yuan, Y.T. Zhu, Mater. Res. Lett. 2 (2014) 185.
[5] K. Lu, Science 345 (2014) 1455.
[6] D. Li, H.N. Chen, H. Xu, Appl. Surf. Sci. 255 (2009) 3811.
[7] N.R. Tao, Z.B. Wang, W.P. Tong, M.L. Sui, J. Lu, K. Lu, Acta Mater. 50 (2002) 4603.
[8] H.W. Zhang, Z.K. Hei, G. Liu, J. Lu, K. Lu, Acta Mater. 51 (2003) 1871.
[9] X. Wu, N. Tao, Y. Hong, G. Liu, B. Xu, J. Lu, K. Lu, Acta Mater. 53 (2005) 681.
[10] L. Zhou, G. Liu, X.L. Ma, K. Lu, Acta Mater. 56 (2008) 78.
[11] K. Wang, N.R. Tao, G. Liu, J. Lu, K. Lu, Acta Mater. 54 (2006) 5281.
[12] J.C. Villegas, L.L. Shaw, Acta Mater. 57 (2009) 5782.
[13] K. Dai, L. Shaw, Mater. Sci. Eng. A 463 (2007) 46.
[14] Y. Ivanisenko, W. Lojkowski, R.Z. Valiev, H.J. Fecht, Acta Mater. 51 (2003) 5555.
[15] A. Ramesh, S.N. Melkote, L.F. Allard, L. Riester, T.R. Watkins, Mater. Sci. Eng. A 390 (2005) 88.
[16] S.V.S.N. Murty, S. Torizuka, K. Nagai, N. Koseki, Y. Kogo, Scr. Mater. 52 (2005) 713.
[17] J.H. Ahn, D. Kwon, J. Mater. Res. 16 (2001) 3170.
[18] S. Swarninathan, M.R. Shankar, S. Lee, J. Hwang, A.H. King, R.F. Kezar, B.C. Rao, T.L. Brown, S. Chandrasekar, W.D. Compton, K.P. Trumble, Mater. Sci. Eng. A 410 (2005) 358.
[19] N. Kamikawa, T. Sakai, N. Tsuji, Acta Mater. 55 (2007) 5873.
[20] R. Blonde, H.L. Chan, N. Allain-Bonasso, B. Bolle, T. Grosdidier, J.A. Lu, J. Alloys Compd. 504 (2010) S410.
[21] W.Y. Chen, W.P. Tong, C.S. He, X. Zhao, L. Zuo, Mater. Sci. Forum 706–709 (2012) 2663.
[22] Q. Wei, K.T. Ramesh, L.J. Kecskes, S.N. Mathaudhu, K.T. Hartwig, Mater. Sci. Forum 579 (2008) 75.
[23] C.S. Barrett, T.B. Massalski, Structure of Metals, McGraw-Hill, New York, 1966.
[24] G. Langford, Metall. Trans. A 8 (1977) 861.